molecules

MDPI

Article

A Formal Rearrangement of Allylic Silanols

Ranjeet A. Dhokale [1], Frederick J. Seidl [2] and Shyam Sathyamoorthi [1,*]

[1] Department of Medicinal Chemistry, University of Kansas, Lawrence, KS 66047, USA; r.dhokale@ku.edu
[2] Independent Researcher, San Bruno, CA 94066, USA; fseidl@alumni.stanford.edu
* Correspondence: ssathyam@ku.edu

Abstract: We show that 1M aqueous HCl/THF or $NaBH_4$/DMF allows for demercurative ring-opening of cyclic organomercurial synthons into secondary silanol products bearing terminal alkenes. We had previously demonstrated that primary allylic silanols are readily transformed into cyclic organomercurials using $Hg(OTf)_2/NaHCO_3$ in THF. Overall, this amounts to a facile two-step protocol for the rearrangement of primary allylic silanol substrates. Computational investigations suggest that this rearrangement is under thermodynamic control and that the di-tert-butylsilanol protecting group is essential for product selectivity.

Keywords: rearrangement; organic synthesis; organic methodology

Citation: Dhokale, R.A.; Seidl, F.J.; Sathyamoorthi, S. A Formal Rearrangement of Allylic Silanols. *Molecules* **2021**, *26*, 3829. https://doi.org/10.3390/molecules26133829

Academic Editors: Roman Dembinski and Igor Alabugin

Received: 8 June 2021
Accepted: 21 June 2021
Published: 23 June 2021

1. Introduction

Rearrangement reactions can be grouped based on mechanism. One category contains true pericyclic reactions, involving a concerted flow of electrons that results in the breaking of a σ bond, simultaneous rearrangement of a π system, and formation of a new σ bond [1]. These rearrangements are effected thermally or through Lewis acid catalysis, and many landmark reactions (Cope [2], Claisen [3], Ireland-Claisen [4–7], Mislow-Evans [8], etc.) fall into this category. The second category contains *formal* sigmatropic processes, where the rearrangement proceeds through a discrete organometallic intermediate. A prominent example of this latter process is the Overman transposition of allylic trichloroacetimidates, which is catalyzed by either mercuric or palladium (II) salts (Scheme 1) [9].

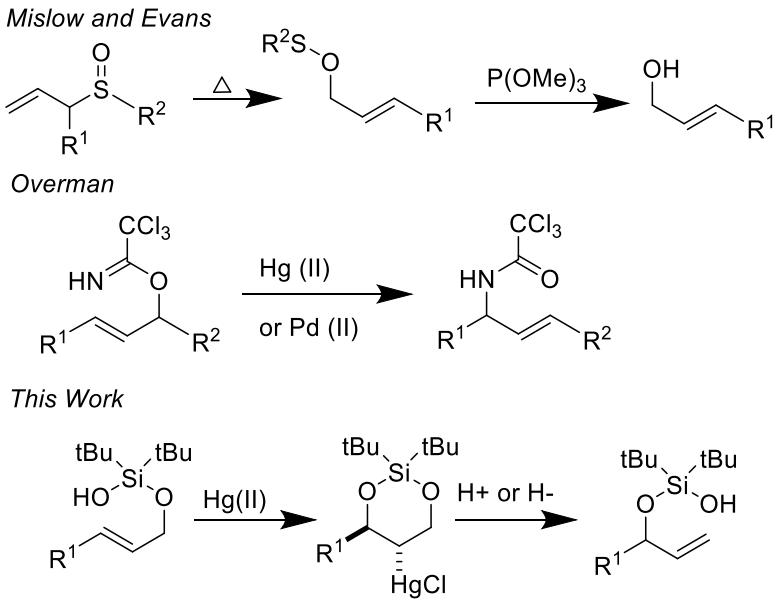

Scheme 1. Known allylic rearrangement reactions inspire this work.

In general, there are few rearrangement reactions of free and protected alcohols (Scheme 2). Pioneering work in this area was accomplished using early transition metal oxo species [10–15] and with Pd (0)/Pd (II) salts [16–19]. Elegant mechanistic studies of these reactions have been conducted by Henry [20], Osborn [21,22], and Grubbs [23,24]. Recent advances have been provided by Floreancig [25–27], Zakarian [28], Lee [29–31], and others [32–35]. Here, we describe a two-step protocol for a rearrangement of allylic silanols. We recently demonstrated a facile transformation of alkenyl silanols into organomercurial synthons [36]. We now show that these organomercurial species can serve as intermediates for a transposition of the allylic silanol substrate.

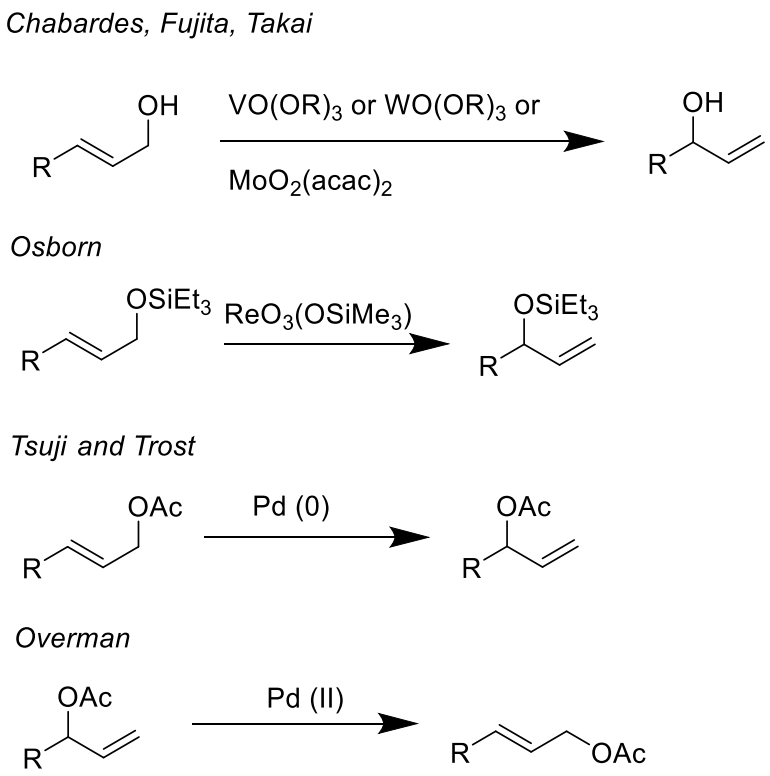

Scheme 2. Few protocols exist for the transposition of free and protected allylic alcohols.

2. Results and Discussion

2.1. Synthetic Investigations

This reaction was discovered serendipitously. To remove unreacted mercuric salts after the cyclization reaction, we explored using a 1M aqueous HCl workup. To our consternation, we recovered starting material with trace amounts of the rearranged product (Scheme 3). Repeating this experiment led to the same result. We thus realized that 1M aqueous HCl was promoting a demercuration reaction leading to starting material regeneration. We wondered if we could change the product distribution to favor the rearranged silanol.

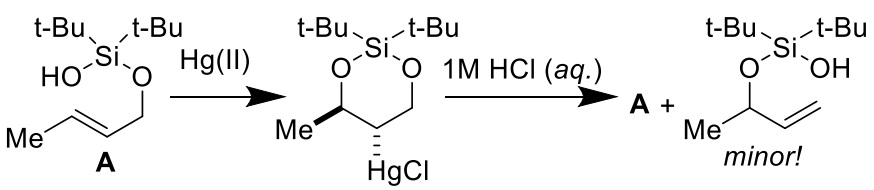

Scheme 3. 1M aqueous HCl promotes an allylic rearrangement reaction.

All attempts to improve the product distribution with **A** were unsuccessful. However, we observed a dramatic improvement upon switching to an organomercurial substrate with a pendant isopropyl group (Table 1, Entry 1). Increasing the reaction temperature gave identical results, but dropping the temperature to 0 °C led to a decrease in yield and selectivity (Table 1, Entries 2–3). Interestingly, treatment with two equivalents of $NaBH_4$ in either DMF or DMSO (Table 1, Entries 4–5) was equally effective in forming rearranged product. Demercuration reactions are known with $NaBH_4$, but generally the products consist of mercury simply substituted with H, OH, or I [35]. There was a profound solvent dependence on outcome with markedly worse reactions observed in MeOH, DMA, and THF (Table 1, Entries 6–8). Switching from $NaBH_4$ to $LiBH_4$ led to marked decomposition of substrate with little discernible product formation (Table 1, Entry 9).

Table 1. Optimization of this allylic rearrangement.

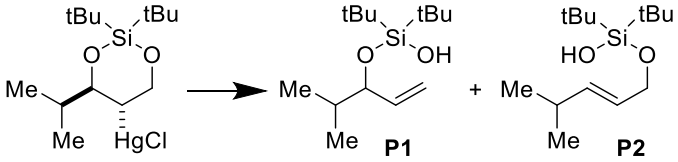

Entry	Reagent	Solvent	Temp.,Time	P1/P2 [a]
1	1M HCl (aqueous)	THF	RT, 30 min	60/20
2	1M HCl (aqueous)	THF	35 °C, 30 min	60/20
3	1M HCl (aqueous)	THF	0 °C, 30 min	50/22
4	$NaBH_4$ (2 equiv)	DMF	RT, 30 min	64/20
5	$NaBH_4$ (2 equiv)	DMSO	RT, 30 min	62/20
6	$NaBH_4$ (2 equiv)	MeOH	RT, 30 min	56/11
7	$NaBH_4$ (2 equiv)	DMA	RT, 30 min	6/4
8	$NaBH_4$ (2 equiv)	THF	RT, 30 min	43/7
9	$LiBH_4$ (2 equiv)	THF	RT, 30 min	10/0

[a] Yield estimated using ^{1}H NMR integration against methyl phenyl sulfone as an internal standard.

The nature of the substituent *trans* to the HgCl group greatly affected the ratio of the two regioisomeric products (Scheme 4). Generally, as the steric bulk of the linear alkyl chain increased, so too did the yield of the terminal alkene regioisomer (Scheme 4, Entries 1–3). With branching at the α carbon (Scheme 4, Entries 4–5) or at the β carbon (Scheme 4, Entry 6), the terminal alkene regioisomer predominated. When there was competition between formation of a terminal alkene and its tri-substituted isomer, the more substituted olefin formed exclusively (Scheme 4, Entry 7).

Our optimized protocols were compatible with a wide array of substrates (Scheme 5). While protocol A (1M aq. HCl/THF) was tested with the majority of substrates, protocol B ($NaBH_4$/DMF) was used for those bearing acid sensitive functionality (Scheme 5, Entries 1–2). In all but one instance (Scheme 5, Entry 10), terminal alkene products were greatly favored; in many cases (Scheme 5, Entries 1–3), these were the exclusive product. A variety of functional groups, including ketals (Scheme 5, Entries 1–2), halogens (Scheme 5, Entry 3; Scheme 5, Entry 6), and alkyl ethers (Scheme 5, Entry 3; Scheme 5, Entry 8) were well tolerated. We were pleased to successfully convert product **40** into a single diastereomer of a protected pentitol using a combination of catalytic $K_2OsO_4 \bullet 2H_2O$ and stoichiometric NMO (Scheme 6).

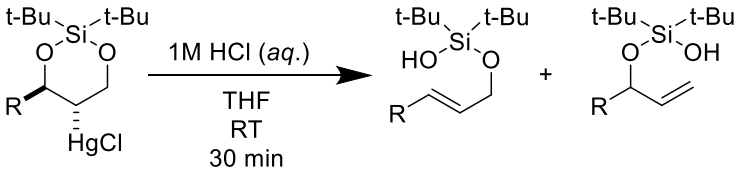

entry[a]	substrate	products[b]	
1	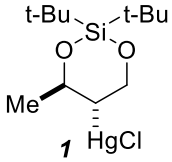	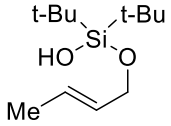	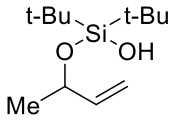
	1	***26* 56%**	***27* 19%**
2	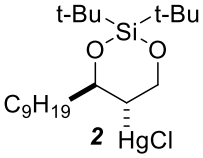	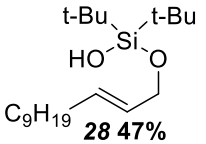	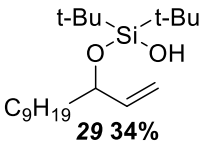
	2	***28* 47%**	***29* 34%**
3	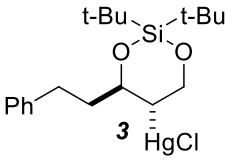	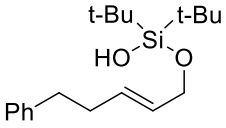	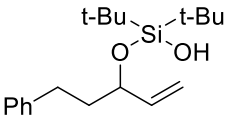
	3	***30* 38%**	***31* 30%**
4	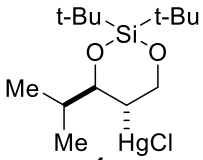	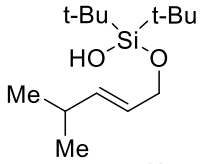	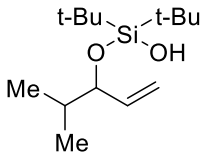
	4	***32* 17%**	***33* 54%**
5	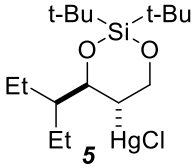	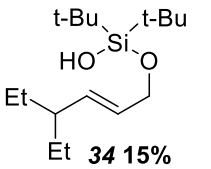	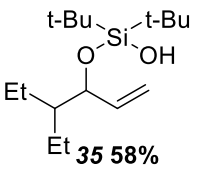
	5	***34* 15%**	***35* 58%**
6	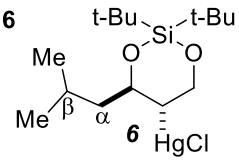	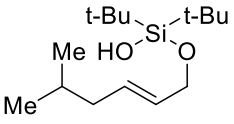	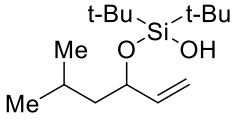
	6	***36* 30%**	***37* 56%**
7	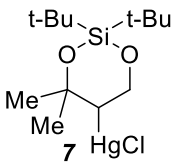	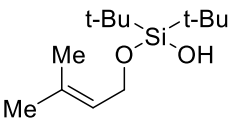	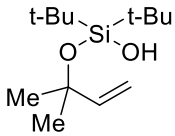
	7	***38* 87%**	***39* 0%**

Scheme 4. Alkene Substituents Markedly Affect Product Distribution. [a] Stereochemistry shown is relative. [b] Isolated yields unless otherwise mentioned.

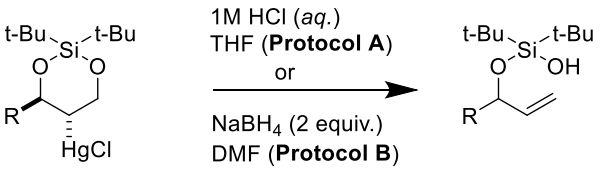

entry[a]	substrate	protocol	product[b]	yield[c]
1	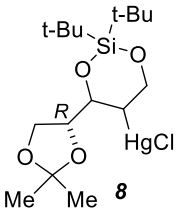	B	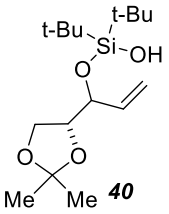	**50%[d]**
2	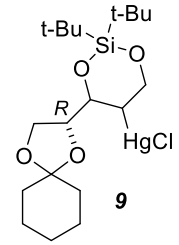	B	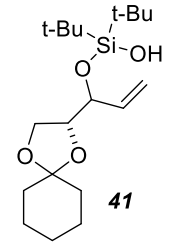	**51%[d]**
3	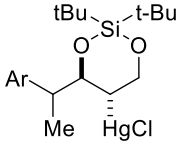	A	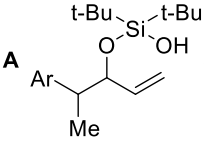	Ar = Ph **75%[d]** *p*ClC$_6$H$_4$ **90%[d]** 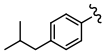 **91%[d]** 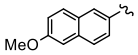 **74%[d]**
4	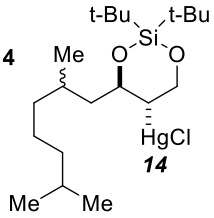	A	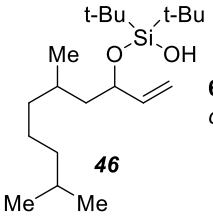	**66% (22%)** *dr = 1:1*
5	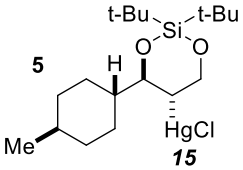	A	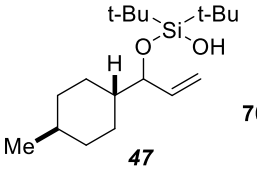	**70% (30%)**
6	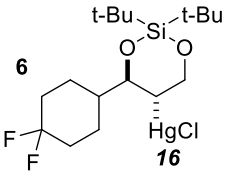	A	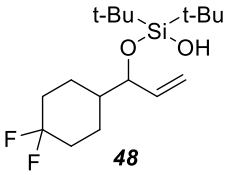	**77% (7%[e])**

Scheme 5. *Cont*.

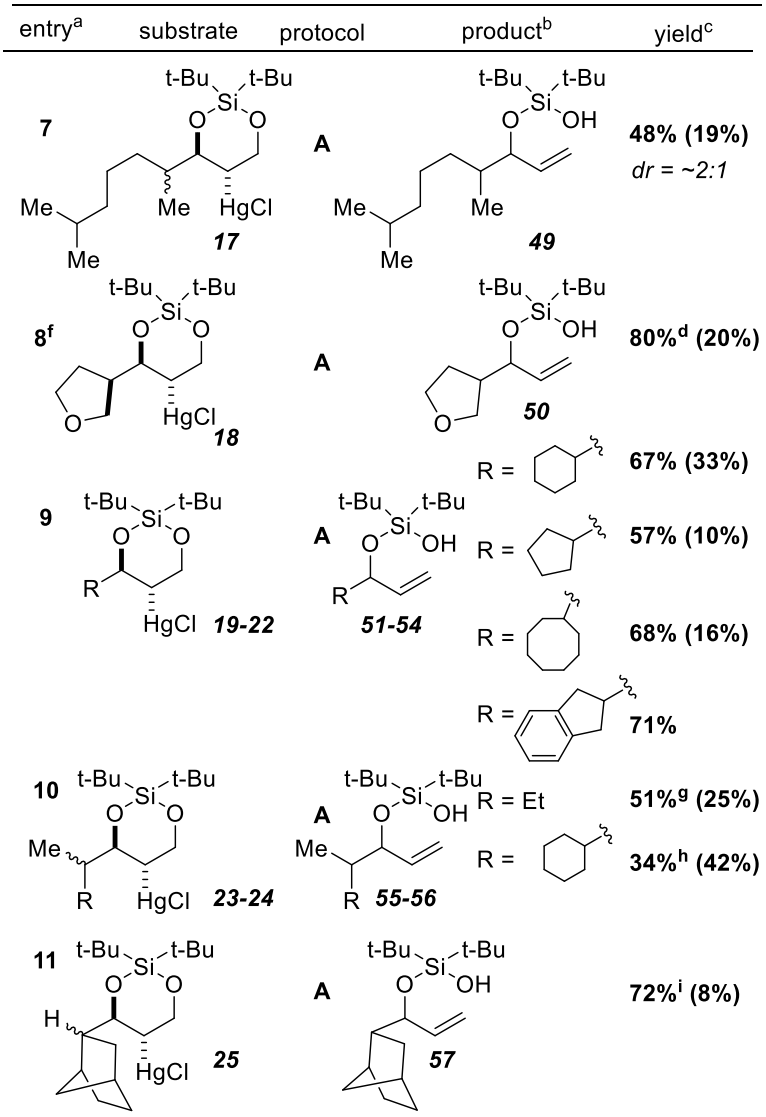

Scheme 5. Substrate Scope. [a] Relative stereochemistry shown unless explicitly indicated. [b] The yield of the internal alkene regio-isomer is shown in parentheses. [c] Isolated yield unless otherwise mentioned. [d] Single diastereomer but relative stereochemistry unassigned. [e] Yield estimated using ^{1}H NMR integration against methyl phenyl sulfone as an internal standard. [f] CCDC number 2052702. [g] dr = ~1.5:1. [h] dr = ~2.5:1. [i] Mixture of diastereomers.

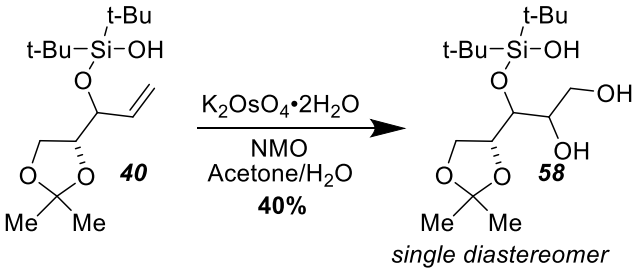

Scheme 6. Product **40** serves as a convenient precursor for a protected pentitol.

2.2. Mechanistic Studies

In order to better understand the observed selectivity, we turned to DFT calculations using the ORCA software package [37,38]. All calculations were performed using the B3LYP functional [39,40] with D3BJ dispersion correction [41,42] using the RIJCOSX ap-

proximation [43]. The def2-TZVP basis set [44] was used, and implicit water solvation was applied using the SMD model [45]. When mercury was present, the def2-ECP [46] was applied automatically. When multiple conformations were possible, a systematic rotor search was performed in Avogadro [47] to identify the lowest energy conformation as a starting point. Further details and atomic coordinates are reported in the Supplementary Materials.

Noting that lower temperature led to lower selectivity for the terminal alkene isomer, we investigated the reaction thermodynamics to determine whether the product distribution was due to equilibrium or kinetics. The simplified reaction mechanism for protocol A is:

$$\text{organomercury} + HCl \rightarrow \text{alkene} + HgCl_2$$

For methyl substrate **1**, the internal alkene **26** is calculated to be preferred by 0.9 kcal/mol (Figure 1). Experimentally, the observed 2.95:1 ratio favoring **26** over **27** corresponds to an expected ΔG of 0.64 kcal/mol according to a Boltzmann population analysis at room temperature:

$$\frac{A}{B} = \exp\frac{E(A) - E(B)}{kT}$$

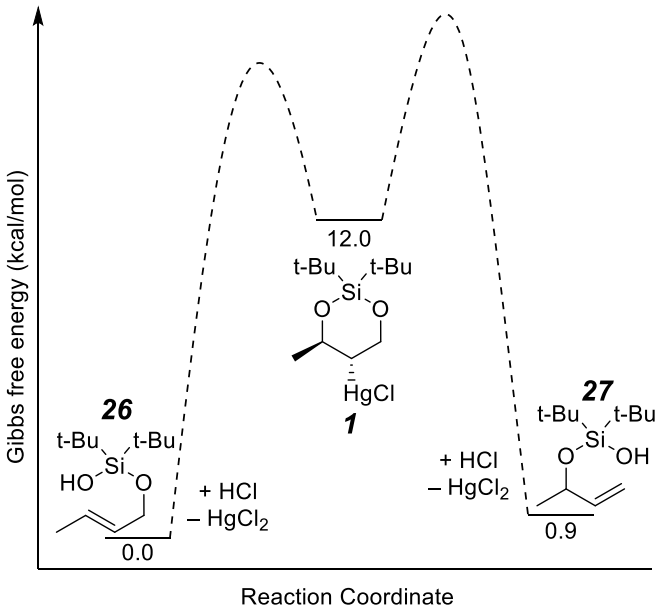

Figure 1. Calculated thermodynamics for methyl substrate **1**.

For isopropyl substrate **4**, the terminal alkene **33** is calculated to be preferred by 0.5 kcal/mol (Figure 2). Experimentally, the observed 3.0:1 ratio favoring **33** over **32** corresponds to an expected ΔG of 0.65 kcal/mol by the same equation above. Because these calculated values align reasonably well with experiment, it appears that the observed reaction selectivity is due to equilibrium thermodynamics.

To better understand this thermodynamic preference, we also modeled the deprotected allylic alcohols. For methyl substrate **1**, the internal alkene (*E*)-2-buten-1-ol was 0.02 kcal/mol higher in Gibbs Free Energy than terminal alkene 3-buten-2-ol or nearly isoenergetic. However, for isopropyl substrate **4**, the internal alkene was 0.28 kcal/mol lower in Gibbs Free Energy than the terminal alkene. Importantly, the molecular dipole of the internal alkene is about 1 Debye larger than the dipole of the terminal alkene in both cases, so implicit water solvation significantly stabilizes the internal alkene with its larger molecular dipole. Because the deprotected allylic alcohols fail to account for the observed selectivity, we conclude that the pendant di-tert-butylsilanol group plays a critical role in determining the thermodynamic selectivity of the reaction.

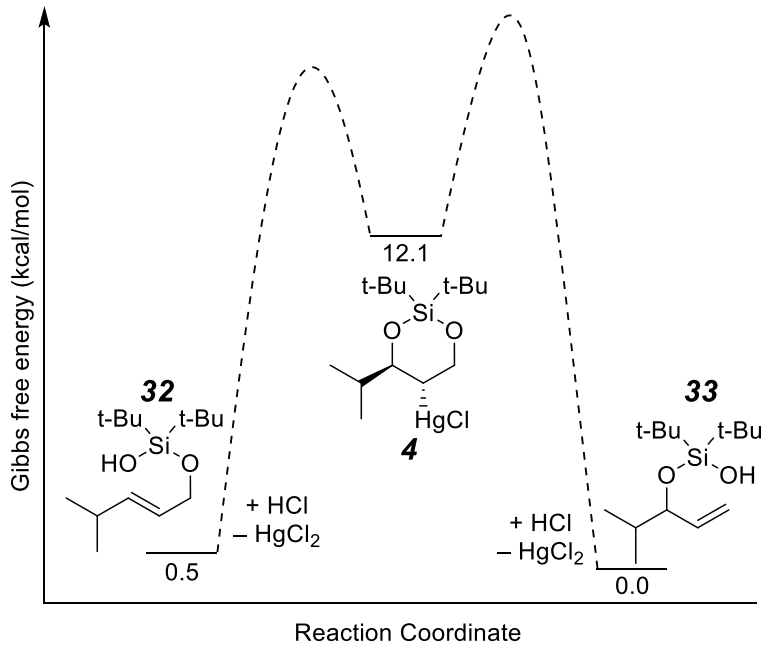

Figure 2. Calculated thermodynamics for isopropyl substrate **4**.

For the reaction to be under thermodynamic control, it must be reversible. The reaction barriers must be low enough to be overcome rapidly at room temperature (<20 kcal/mol). We began by modeling mercuronium rearrangements based on literature precedent for similar reactions [48]. An intrinsic reaction coordinate (IRC) calculation from the rearrangement transition state leading to the major terminal alkene isomer **33** is included below (Figure 3). Starting from **4**, the silanol oxygen is protonated to form **59**, then the C–O bond is broken with concomitant mercuronium formation. The transition state **60** is very late and product-like, and the potential energy surface in this region is very flat, complicating analysis. A stationary point could not be located for the discrete mercuronium product **61**. Instead, **61** spontaneously engages in a 5-exo ring closure to reversibly re-form an isomeric alkylmercury species. This pathway is ultimately not productive as no side products of this type are isolated experimentally. Most likely, mercuronium **61** is very short-lived and is rapidly abstracted by chloride to form $HgCl_2$, which was not modeled. The overall calculated reaction pathway is exothermic by 12 kcal/mol and has an 8 kcal/mol barrier from SM **59** to TS **60**. It follows that the reverse reaction starting from alkene **33** should have a barrier of about 20 kcal/mol, which establishes the reaction as feasibly reversible at room temperature.

The same transition state analysis was performed for the pathway leading to the minor internal alkene product **32**, for which a reaction barrier of only 5.1 kcal/mol was observed. Were this reaction under kinetic control, **32** would be overwhelmingly preferred over **33** with a $\Delta\Delta G^{\ddagger}$ of over 3 kcal/mol. This preference for a more substituted mercuronium ion is expected from Markovnikov selectivity rules due to the partial carbocation character of the mercuronium ion. Overall, for methyl organomercury substrate **1**, the internal alkene **26** is favored by both thermodynamics and kinetics, whereas for isopropyl organomercury substrate **4**, kinetics favors the internal alkene **32**, and thermodynamics favors the terminal alkene **33**.

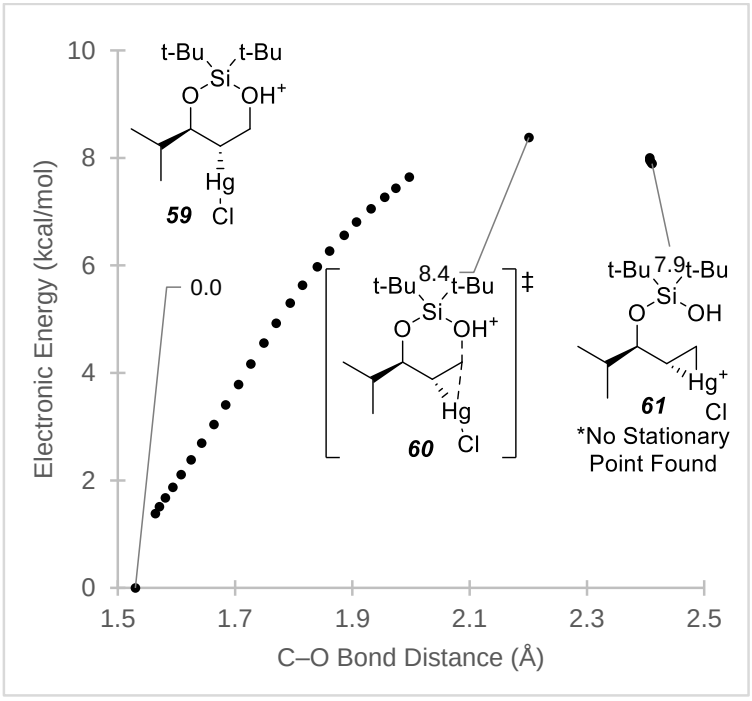

Figure 3. Mercuronium rearrangement of isopropyl substrate 4 (IRC calculation from the transition state).

3. Materials and Methods

All reagents were obtained commercially unless otherwise noted. Solvents were purified by passage under 10 psi N_2 through activated alumina columns. Infrared (IR) spectra were recorded on a Thermo Scientific™ Nicolet™ iS™5 FT-IR Spectrometer (Waltham, MA, USA); data are reported in frequency of absorption (cm^{-1}). NMR spectra were recorded on a Bruker Avance (Billerica, MA, USA) 400 operating at 400 and 100 MHz. 1H NMR spectra were recorded at 400 MHz.

Data were recorded as: chemical shift in ppm referenced internally using residue solvent peaks, multiplicity (s = singlet, d = doublet, t = triplet, q = quartet, m = multiplet or overlap of nonequivalent resonances), integration, coupling constant (Hz). ^{13}C NMR spectra were recorded at 100 MHz. Exact mass spectra were recorded using an electrospray ion source (ESI) either in positive mode or negative mode and with a time-of-flight (TOF) analyzer on a Waters LCT PremierTM mass spectrometer (Milford, MA, USA) and are given in m/z. TLC was performed on pre-coated glass plates (Merck) and visualized either with a UV lamp (254 nm) or by dipping into a solution of $KMnO_4$–K_2CO_3 in water followed by heating. Flash chromatography was performed on silica gel (230–400 mesh). Reversed phase HPLC was performed on a Hamilton PRP-1.7 μm, 21.2 × 250 mm, C18 column. $Hg(OTf)_2$ was purchased from either Alfa Aesar (Ward Hill, MA, USA) or Strem Chemicals (Newburyport, MA, USA). Di-tert-butylsilyl Bis(trifluoromethanesulfonate) was purchased from either TCI America (Portland, OR, USA) or from Sigma-Aldrich (St. Louis, MO, USA).

4. Conclusions

In summary, we presented a two-step protocol for the rearrangement of allylic silanols. We had previously demonstrated that primary allylic silanols are readily transformed into cyclic organomercurials using $Hg(OTf)_2/NaHCO_3$ in THF. Here, we show that using either 1M aqueous HCl/THF or $NaBH_4$/DMF allows for demercurative ring-opening to form secondary silanol products bearing terminal alkenes. Computational investigations suggest that this rearrangement is under thermodynamic control and that the di-tert-butylsilanol protecting group is essential for product selectivity.

Supplementary Materials: The following are available online: I. General Considerations, II. Characterization of Previously Unreported Substrates, III. General Procedures for Allylic Rearrangement Reactions, IV. Characterization of Allylic Rearrangement Products, V. Dihydroxylation Procedure, VI. Crystal Structure Data for **18** (CCDC: 2052702), VII. Computational Procedures and Atomic Coordinates, VIII. NMR Spectra.

Author Contributions: S.S. conceived the project. S.S., R.A.D., and F.J.S. performed experiments. S.S. and F.J.S. wrote the manuscript. All authors have read and agreed to the published version of the manuscript.

Funding: This work was supported by start-up funding provided jointly by the University of Kansas Office of the Provost and the Department of Medicinal Chemistry and an NIH COBRE Chemical Biology of Infectious Diseases Research Project Grant (P20GM113117).

Institutional Review Board Statement: Not applicable.

Informed Consent Statement: Not applicable.

Data Availability Statement: Requests for data not shown in the supporting information should be directed to the corresponding author (ssathyam@ku.edu).

Acknowledgments: We thank Victor Day (University of Kansas) for X-ray crystallography analysis.

Conflicts of Interest: The authors declare no conflict of interest.

Sample Availability: Upon request to the corresponding author (ssathyam@ku.edu).

References

1. Greer, E.M.; Cosgriff, C.V. Reaction mechanisms: Pericyclic reactions. *Annu. Rep. Sect. B (Org. Chem.)* **2013**, *109*, 328–350. [CrossRef]
2. Graulich, N. The Cope rearrangement—the first born of a great family. *WIREs Comput. Mol. Sci.* **2011**, *1*, 172–190. [CrossRef]
3. Martín Castro, A.M. Claisen Rearrangement over the Past Nine Decades. *Chem. Rev.* **2004**, *104*, 2939–3002. [CrossRef] [PubMed]
4. Ito, H.; Taguchi, T. Asymmetric Claisen rearrangement. *Chem. Soc. Rev.* **1999**, *28*, 43–50. [CrossRef]
5. Kesava Reddy, N.; Chandrasekhar, S. Total Synthesis of (−)-α-Kainic acid via Chirality Transfer through Ireland–Claisen Rearrangement. *J. Org. Chem.* **2013**, *78*, 3355–3360. [CrossRef]
6. Qin, Y.-c.; Stivala, C.E.; Zakarian, A. Acyclic Stereocontrol in the Ireland–Claisen Rearrangement of α-Branched Esters. *Angew. Chem. Int. Ed.* **2007**, *46*, 7466–7469. [CrossRef]
7. Fulton, T.J.; Cusumano, A.Q.; Alexy, E.J.; Du, Y.E.; Zhang, H.; Houk, K.N.; Stoltz, B.M. Global Diastereoconvergence in the Ireland–Claisen Rearrangement of Isomeric Enolates: Synthesis of Tetrasubstituted α-Amino Acids. *J. Am. Chem. Soc.* **2020**, *142*, 21938–21947. [CrossRef]
8. Li, J.J. Mislow–Evans rearrangement. In *Name Reactions: A Collection of Detailed Mechanisms and Synthetic Applications*; Li, J.J., Ed.; Springer: Berlin/Heidelberg, Germany, 2009; pp. 363–364.
9. Overman, L.E. Molecular rearrangements in the construction of complex molecules. *Tetrahedron* **2009**, *65*, 6432–6446. [CrossRef]
10. Chabardes, P.; Kuntz, E.; Varagnat, J. Use of oxo-metallic derivatives in isomerisation: Reactions of unsaturated alcohols. *Tetrahedron* **1977**, *33*, 1775–1783. [CrossRef]
11. Volchkov, I.; Lee, D. Recent developments of direct rhenium-catalyzed [1,3]-transpositions of allylic alcohols and their silyl ethers. *Chem. Soc. Rev.* **2014**, *43*, 4381–4394. [CrossRef]
12. Matsubara, S.; Takai, K.; Nozaki, H. Isomerization of primary allylic alcohols to tertiary ones by means of $Me_3SiOOSiMe_3$-$VO(acac)_2$ catalyst. *Tetrahedron Lett.* **1983**, *24*, 3741–3744. [CrossRef]
13. Hosogai, T.; Fujita, Y.; Ninagawa, Y.; Nishida, T. Selective Allylic Rearrangement with Tungsten Catalyst. *Chem. Lett.* **1982**, *11*, 357–360. [CrossRef]
14. Belgacem, J.; Kress, J.; Osborn, J.A. On the allylic rearrangements in metal oxo complexes: Mechanistic and catalytic studies on $MoO_2(allyloxo)_2(CH_3CN)_2$ and analogous complexes. *J. Am. Chem. Soc.* **1992**, *114*, 1501–1502. [CrossRef]
15. Narasaka, K.; Kusama, H.; Hayashi, Y. Rearrangement of Allylic and Propargylic Alcohols Catalyzed by the Combined Use of tetrabutylammonium perrhenate (VII) and p-toluenesulfonic acid. *Tetrahedron* **1992**, *48*, 2059–2068. [CrossRef]
16. Tsuji, J. Dawn of organopalladium chemistry in the early 1960s and a retrospective overview of the research on palladium-catalyzed reactions. *Tetrahedron* **2015**, *71*, 6330–6348. [CrossRef]
17. Trost, B.M.; Van Vranken, D.L. Asymmetric Transition Metal-Catalyzed Allylic Alkylations. *Chem. Rev.* **1996**, *96*, 395–422. [CrossRef] [PubMed]
18. Overman, L.E. Mercury(II)- and Palladium(II)-Catalyzed [3,3]-Sigmatropic Rearrangements [New Synthetic Methods (46)]. *Angew. Chem. Int. Ed. Engl.* **1984**, *23*, 579–586. [CrossRef]
19. Overman, L.E.; Knoll, F.M. Palladium (II)—Catalyzed rearrangement of allylic acetates. *Tetrahedron Lett.* **1979**, *20*, 321–324. [CrossRef]

20. Henry, P.M. Palladium(II)-catalyzed exchange and isomerization reactions. III. Allylic esters isomerization in acetic acid catalyzed by palladium(II) chloride. *J. Am. Chem. Soc.* **1972**, *94*, 5200–5206. [CrossRef]
21. Belgacem, J.; Kress, J.; Osborn, J.A. Catalytic oxidation and ammoxidation of propylene. Modelling studies on well-defined molybdenum complexes. *J. Mol. Catal.* **1994**, *86*, 267–285. [CrossRef]
22. Bellemin-Laponnaz, S.; Gisie, H.; Le Ny, J.P.; Osborn, J.A. Mechanistic Insights into the Very Efficient [ReO3OSiR3]-Catalyzed Isomerization of Allyl Alcohols. *Angew. Chem. Int. Ed. Engl.* **1997**, *36*, 976–978. [CrossRef]
23. Morrill, C.; Beutner, G.L.; Grubbs, R.H. Rhenium-Catalyzed 1,3-Isomerization of Allylic Alcohols: Scope and Chirality Transfer. *J. Org. Chem.* **2006**, *71*, 7813–7825. [CrossRef] [PubMed]
24. Morrill, C.; Grubbs, R.H. Highly Selective 1,3-Isomerization of Allylic Alcohols via Rhenium Oxo Catalysis. *J. Am. Chem. Soc.* **2005**, *127*, 2842–2843. [CrossRef] [PubMed]
25. Xie, Y.; Floreancig, P.E. Stereoselective heterocycle synthesis through a reversible allylic alcohol transposition and nucleophilic addition sequence. *Chem. Sci.* **2011**, *2*, 2423–2427. [CrossRef]
26. Jung, H.H.; Seiders Ii, J.R.; Floreancig, P.E. Oxidative Cleavage in the Construction of Complex Molecules: Synthesis of the Leucascandrolide A Macrolactone. *Angew. Chem. Int. Ed.* **2007**, *46*, 8464–8467. [CrossRef]
27. Xie, Y.; Floreancig, P.E. Cascade Approach to Stereoselective Polycyclic Ether Formation: Epoxides as Trapping Agents in the Transposition of Allylic Alcohols. *Angew. Chem. Int. Ed.* **2013**, *52*, 625–628. [CrossRef]
28. Herrmann, A.T.; Saito, T.; Stivala, C.E.; Tom, J.; Zakarian, A. Regio- and Stereocontrol in Rhenium-Catalyzed Transposition of Allylic Alcohols. *J. Am. Chem. Soc.* **2010**, *132*, 5962–5963. [CrossRef]
29. Lee, D.; Volchkov, I. Chapter 7—Regio- and Stereoselective Metal-Catalyzed Reactions and Their Application to a Total Synthesis of (−)-Dactylolide. In *Strategies and Tactics in Organic Synthesis*; Harmata, M., Ed.; Academic Press: Cambridge, MA, USA, 2012; Volume 8, pp. 171–197.
30. Volchkov, I.; Park, S.; Lee, D. Ring Strain-Promoted Allylic Transposition of Cyclic Silyl Ethers. *Org. Lett.* **2011**, *13*, 3530–3533. [CrossRef]
31. Volchkov, I.; Lee, D. Asymmetric Total Synthesis of (−)-Amphidinolide V through Effective Combinations of Catalytic Transformations. *J. Am. Chem. Soc.* **2013**, *135*, 5324–5327. [CrossRef]
32. Zheng, H.; Lejkowski, M.; Hall, D.G. Mild and selective boronic acid catalyzed 1,3-transposition of allylic alcohols and Meyer–Schuster rearrangement of propargylic alcohols. *Chem. Sci.* **2011**, *2*, 1305–1310. [CrossRef]
33. Mandal, A.K.; Schneekloth, J.S.; Kuramochi, K.; Crews, C.M. Synthetic Studies on Amphidinolide B1. *Org. Lett.* **2006**, *8*, 427–430. [CrossRef]
34. Trost, B.M.; Toste, F.D. Enantioselective Total Synthesis of (−)-Galanthamine. *J. Am. Chem. Soc.* **2000**, *122*, 11262–11263. [CrossRef]
35. Shinde, A.H.; Sathyamoorthi, S. Tethered Silanoxymercuration of Allylic Alcohols. *Org. Lett.* **2020**, *22*, 8665–8669. [CrossRef] [PubMed]
36. Bonini, C.; Campaniello, M.; Chiummiento, L.; Videtta, V. Stereoselective synthesis of versatile 2-chloromercurium-3,5-syn-dihydroxy esters via intramolecular oxymercuration. *Tetrahedron* **2008**, *64*, 8766–8772. [CrossRef]
37. Neese, F. The ORCA program system. *WIREs Comput. Mol. Sci.* **2012**, *2*, 73–78. [CrossRef]
38. Neese, F. Software update: The ORCA program system, version 4.0. *WIREs Comput. Mol. Sci.* **2018**, *8*, e1327. [CrossRef]
39. Becke, A.D. A new mixing of Hartree–Fock and local density-functional theories. *J. Chem. Phys.* **1993**, *98*, 1372–1377. [CrossRef]
40. Lee, C.; Yang, W.; Parr, R.G. Development of the Colle-Salvetti correlation-energy formula into a functional of the electron density. *Phys. Rev. B* **1988**, *37*, 785–789. [CrossRef]
41. Grimme, S.; Antony, J.; Ehrlich, S.; Krieg, H. A consistent and accurate ab initio parametrization of density functional dispersion correction (DFT-D) for the 94 elements H-Pu. *J. Chem. Phys.* **2010**, *132*, 154104. [CrossRef]
42. Grimme, S.; Ehrlich, S.; Goerigk, L. Effect of the damping function in dispersion corrected density functional theory. *J. Comput. Chem.* **2011**, *32*, 1456–1465. [CrossRef]
43. Weigend, F. Accurate Coulomb-fitting basis sets for H to Rn. *Phys. Chem. Chem. Phys.* **2006**, *8*, 1057–1065. [CrossRef]
44. Weigend, F.; Ahlrichs, R. Balanced basis sets of split valence, triple zeta valence and quadruple zeta valence quality for H to Rn: Design and assessment of accuracy. *Phys. Chem. Chem. Phys.* **2005**, *7*, 3297–3305. [CrossRef] [PubMed]
45. Marenich, A.V.; Cramer, C.J.; Truhlar, D.G. Universal Solvation Model Based on Solute Electron Density and on a Continuum Model of the Solvent Defined by the Bulk Dielectric Constant and Atomic Surface Tensions. *J. Phys. Chem. B* **2009**, *113*, 6378–6396. [CrossRef]
46. Andrae, D.; Häußermann, U.; Dolg, M.; Stoll, H.; Preuß, H. Energy-adjustedab initio pseudopotentials for the second and third row transition elements. *Theor. Chim. Acta* **1990**, *77*, 123–141. [CrossRef]
47. Hanwell, M.D.; Curtis, D.E.; Lonie, D.C.; Vandermeersch, T.; Zurek, E.; Hutchison, G.R. Avogadro: An advanced semantic chemical editor, visualization, and analysis platform. *J. Cheminform.* **2012**, *4*, 17. [CrossRef] [PubMed]
48. Bordwell, F.G.; Douglass, M.L. Reduction of Alkylmercuric Hydroxides by Sodium Borohydride. *J. Am. Chem. Soc.* **1966**, *88*, 993–999. [CrossRef]